Available online at www.sciencedirect.com
SCIENCE DIRECT
Polymer 46 (2005) 6657–6665
polymer
www.elsevier.com/locate/polymer

In situ generation of nanoparticulate lanthanum(III) oxide-polyimide films: characterization of nanoparticle formation and resulting polymer properties

E. Espuche[a], L. David[a], C. Rochas[b], J.L. Afeld[c], J.M. Compton[c], D.W. Thompson[c], D. Scott Thompson[c,1], D.E. Kranbuehl[c,*]

[a]*Laboratoire des Matériaux Polymères et des Biomatériaux, UMR 5627, Bât. ISTIL, 15 Bd A. Latarget, 69622 Villeurbanne Cedex, France*
[b]*Laboratoire de Spectroscopie Physique (LSP), Université Joseph Fourier, UMR CNRS 5588, 140 Avenue de la Physique BP 87, 38402 Saint-Martin d'Hères, France*
[c]*Departments of Chemistry and Applied Science, College of William and Mary, Williamsburg, VA 23187, USA*

Available online 22 June 2005

Abstract

An in situ and single-step route to creating a uniform dispersion of lanthanum(III) oxide nanoparticles in a polyimide is described. The process of thermally evolving, from the diaquotris(2,4-pentanedionato)lanthanum(III) complex, to a homogeneous dispersion of lanthanum(III) oxide nanoparticles within a 6FDA/1,3(3)-APB polyimide matrix has been characterized. The report also describes the resulting changes in the final properties of the hybrid material relative to the neat polyimide. Characterization techniques include dielectric spectroscopy, small angle X-ray scattering, X-ray photoelectron spectroscopy, and gas permeability.

Keywords: Nanoparticles; Polyimide films; Gas permeability

1. Introduction

The incorporation of inorganic materials, e.g. metal oxides (e.g. Si, Ti, La, Ho, Gd, etc.) [1–8], exfoliated silicate sheet minerals [9–25], carbon nanotubes [26–31], and passive metals (e.g. Ag, Pd) [32–39], as nanometer-sized particles of low weight and volume fractions into polyimides has been shown to significantly enhance a range of properties including glass transition temperature, coefficient of thermal expansion, thermal conductivity, gas permeability, tensile modulus and strength, dielectric phenomena, optical reflectivity, and non-linear optical effects. The focus of most of these studies was to demonstrate the enhancement of a nanoparticulate inorganic phase on a physical property of the hybrid material. Much of this work has focused on hybrid materials derived from organically modified montmorillonites which are difficult systems to fully understand because of the complex electrostatic interactions at the surface of the silicate sheet particles, exfoliation/delamination challenges, and the residues left after processing from the very large organic ammonium or phosphonium cations. In earlier papers it was shown that the linear coefficient of thermal expansion (CTE) of fluorine-containing polyimide-lanthanum(III) oxide composites is lowered by as much as 40% coupled with an increase in the tensile modulus [4–6]. These observed enhancements of the CTE and modulus in nanocomposite Ln_2O_3-6FDA/1,3(3)-APB (2,2-bis(3,4-dicarboxypheny)-hexafluoropropane dianhydride/1,3-bis(3-aminophenoxy)-benzene—Fig. 1) films (Ln = La, Gd, and Ho) were quantitatively very similar to the parallel system of montmorillonites in PMDA/ODA (pyromellitic dianhydride/oxydianiline).

The work reported herein focuses on characterizing La_2O_3 nanoparticle formation in 6FDA/1,3(3)-APB during thermal curing and investigating the resulting effects on the

* Corresponding author. Tel.: +1 757 221 2542; fax: +1 757 221 2715.
E-mail address: dekran@wm.edu (D.E. Kranbuehl).
[1] Present address: 3 M Corporation, Electronics and Inorganic Materials Technology Center, St Paul, MN 55144-1000, USA.

0032-3861/$ - see front matter © 2005 Elsevier Ltd. All rights reserved.
doi:10.1016/j.polymer.2005.05.020

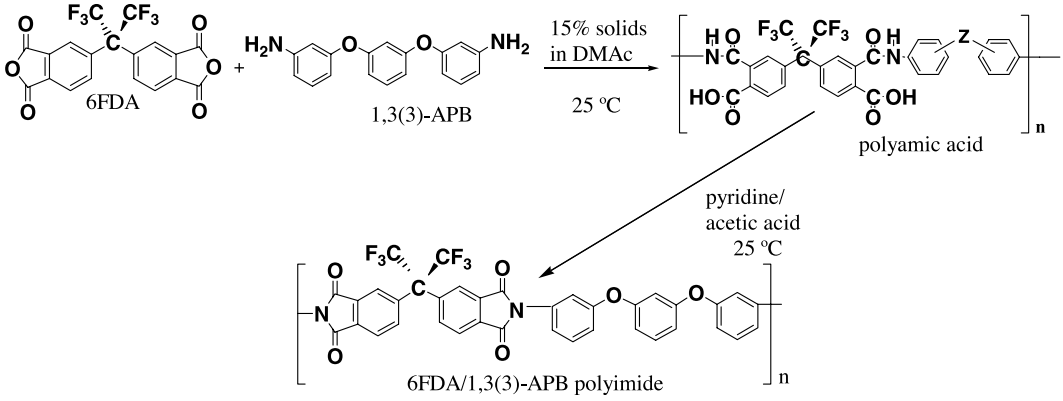

Fig. 1. Preparative scheme for 6 FDA/1,3(3)-APB.

gas permeability properties of the modified nanocomposite polymer. The synthesis of the La_2O_3 nanoparticle-polyimide hybrid films of this paper utilizes a novel in situ method that we have recently elaborated [4–8,40]. This method is distinctive in that it is an in situ and single-step route dispersing metal-oxo nanoparticles uniformly throughout the polymer matrix. Polyimides are significant to study due to their thermal stability (at and above 300 °C) and because of the extensive permeability studies conducted on this family of polymers due to their innate gas selectivity. Moreover, 6FDA/1,3(3)-APB was chosen because fluorinated polyimides are soluble in a range of solvents removing the need for thermal imidization, thereby uncomplicating the final results. The choice to incorporate lanthanide(III) oxides species into the polyimide was based on the enhanced tendency of lanthanide(III) complexes with oxo ligands such as alkoxides and beta-diketonates to undergo thermal and hydrolytic transformations to polynuclear $M_x(\mu_x\text{–O})$ cores which then can continue on to a final M_2O_3 phase.

Size, shape, and chemical identity of the nanoparticle and interaction of the nanoparticles with the polymeric matrix can affect significantly the final properties of a hybrid material. The ongoing objective of our research is to develop a fundamental understanding of hybrid materials containing inorganic nanoparticles embedded in an organic macromolecular matrix in terms of: (1) the formation and intrinsic properties of the nanoparticles and (2) the structure and properties inherent to the polymer. First, this report focuses on characterizing the process of thermally evolving, from the diaquotris(2,4-pentanedionato)lanthanum(III) complex [41] to a homogeneous dispersion of lanthanum(III) oxide nanoparticles within a 6FDA/1,3(3)-APB polyimide matrix. Second the report describes the resulting changes in the final properties of the hybrid material relative to the neat polyimide. Characterization techniques include dielectric spectroscopy, small angle X-ray scattering (SAXS), X-ray photoelectron spectroscopy, and gas permeability.

2. Experimental

2.1. Materials

2,2-Bis(3,4-dicarboxypheny)hexafluoropropane dianhydride (6FDA) was obtained from Hoechst Celanese and vacuum dried for 17 h at 110 °C. 1,3-Bis(3-aminophenoxy) benzene (1,3(3)-APB) was purchased from National Starch and used as received. 2,4-Pentanedione and lanthanum(III) oxide were obtained form Fisher and Aldrich, respectively. DMAc (HPLC grade) was purchased from Aldrich and stored over 4A molecular sieves.

As outlined in Fig. 1 imidized 6FDA/1,3(3)-APB was prepared by the addition of 6FDA (0.5% molar excess) to a DMAc solution of 1,3(3)-APB to first prepare the poly(amic acid) at 15% solids (w/w). The reaction mixture was stirred at the ambient temperature for 7 h. The inherent viscosity of the poly(amic acid) was 1.4 dL/g at 35 °C. This amic acid precursor was chemically imidized at room temperature in an equal molar ratio acetic acid–pyridine solution, the pyridine and acetic acid each being three times the moles of diamine monomer. The polyimide was then precipitated in water, washed thoroughly with deionized water, and vacuum dried at 200 °C for 20 h after which no odor of any solvent was detectable. The inherent viscosity of the polyimide in DMAc was 0.81 dL/g at 35 °C. M_n and M_w were determined by GPC to be 86,000 and 289,000 g/mol, respectively.

2.2. Preparation of the diaquotris(2,4-pentanedionato) lanthanum(III) nanoparticle precursor complex

The title complex was made following the approach of Pope et al. [42], Stites et al. [43], and Phillips et al. [41]. Redistilled 2,4-pentanedione (50 mL) was combined with 15 M ammonia and water until the diketone went into solution as the ammonium salt. Lanthanum(III) chloride was prepared by dissolving lanthanum(III) oxide in 6 M hydrochloric acid. The pH was adjusted to 5.0 with sodium hydroxide. The ammonia solution of 2,4-pentanedione was

added drop wise to the stirring lanthanum(III) chloride solution. The pH of this final solution was allowed to rise to six and held constant at this value. The solution was stirred for 24 h during which time the colorless crystalline complex formed. The product was filtered, washed twice with deionized water, and dried in air for 4 h after which it was recrystallized from 95% ethanol. The final crystals were dried in air at the ambient temperature.

2.3. Preparation of oxo-lanthanum(III)-polyimide films

Metal doped 6FDA/1,3(3)-APB polyimide solutions were prepared by first dissolving the metal complex in DMAC and then adding solid imide powder to give a 15% solids (excluding the lanthanum(III) additive) solution. The solutions were stirred 2–4 h to dissolve all of the polyimide. The clear complex-doped resins were cast as films onto soda lime glass plates using a doctor blade set to give cured films ca. 25 μm in thickness. The films were allowed to sit for 15 h at room temperature in flowing air at 5% humidity which resulted in a film that was tact free. The films then were cured in a forced air oven and removed from the plate by soaking in warm deionized water. The cure cycle for films used in permeability studies was 100 °C for 1 h, 30 min to 200 °C for 1 h; 30 min to 300 °C for 1 h. This cure cycle allowed minimization of the amount of residual solvent in the film. The films for SAXS analysis were cured as follows: 30 min ramp from room temperature to 100 °C; hold for 1 h at 100 °C; 100–300 °C over a 2 h linear ramp; hold at 300 °C for 1 h.

All of the results in this report concern films prepared at a molar concentration of polymer repeat unit-to-metal of 5:1, corresponding to 4.4 wt% of La_2O_3 in the polyimide (ca. 1.1 vol% assuming the La_2O_3 density to be 6.3 g/cm^3 with the 6FDA/1,3(3)-APB density at 1.43 g/cm^3). For gas permeability, the study was enlarged to three polymer repeat unit-to-metal compositions 5:1, 7:1 and 12:1 corresponding to a weight metal content of 4.64, 3.02 and 1.79%, respectively.

2.4. Characterization of the formation of La_2O_3 nanoparticles and their final morphology

The temperature–time dependence of the growth of the La_2O_3 nanoparticles was followed by dielectric analysis (using a HP 4192A LCR meter and an interdigitated sensor composed of gold electrodes patterned on quartz) and by modulated differential scanning calorimetry (using a TA instruments 2920 apparatus). Thermal gravimetric analysis of the decomposition of diaquotris(2,4-pentanedionato) lanthanum(III) has been previously reported [6].

The evolution of La_2O_3 nanoparticles in the 6FDA/1,3(3)-APB polyimide matrix was followed by SAXS experiments performed at the European Synchrotron Radiation facility (Grenoble, France) on BM2-D2AM beamline. A CCD camera was used (Ropper Scientific) and scattering diagrams are obtained after radial averages around the image center (location of the center of the incident beam). The data were collected in about 100 s, at an incident photon energy of 16 keV, and using silver behenate as a q-range calibration standard. The contribution of empty cell was subtracted by monitoring the transmitted intensity by means of an 8 μm Kapton foil tilted at 45° and a photomultiplicator in the first part of the evacuated tube.

2.5. Characterization of physical properties

Gas permeation experiments were carried out at 20 °C under an upstream pressure equal to 3 bar for H_2 and CO_2, two gases differing by their size and interaction capacity. The permeation cell consisted of two compartments separated by the studied membrane. A preliminary high vacuum desorption was realized before each experiment. The 3 bar gas pressure was then applied in the upstream compartment and the pressure variations in the downstream compartment were measured as a function of time with a datametrics pressure sensor. The permeability coefficient P expressed in barrer unit (1 Barrer $= 10^{-10}$ cm^3_{STP} cm cm^{-2} s^{-1} cm^{-1}_{Hg}) was calculated from the slope of the steady state line and the diffusion coefficient D was deduced from the time lag provided by the extrapolation of this straight line on the time axis.

We have also studied the effects of the nanoparticles on the glass transition temperature, the modulus and coefficient of thermal expansion.

3. Results and discussion

3.1. Synthesis considerations for lanthanum(III) oxide-6FDA/1,3(3)-APB nanocomposite films

To achieve nanoparticles it is imperative that the La(III) additive is soluble in solutions of imidized 6FDA/1,3(3)-APB and in the solvent free polyimide which develops as the solvent dimethylacetamide (DMAc) is lost in the cure cycle. The $[La(acac)_3(H_2O)_2]$ complex is soluble in DMAc, and it remains dispersed in the uncured tact-free and solvent-free polymer films, which is apparent from the uniform, translucent nature of the films after drying at ambient temperature. During thermal treatment of the complex-doped films no phase separation occurs. Films were typically prepared at a molar concentration of polymer repeat unit-to-metal of 5:1; concentrations of the complex greater than ca. 3:1 give films which fractured on handling.

$[La(acac)_3(H_2O)_2]$ was chosen as the inorganic precursor to a metal-oxo phase for several reasons. First, La(III) is a metal ion which has a single stable tervalent oxidation state with a very large crystal radius of 117 pm [44]. Second, coordination numbers for La(III) complexes are commonly eight and nine [45]. Thus, in La(III) we have a metal ion which has an expanded coordination sphere and is a hard

Lewis acid, both allowing for enhanced binding to polymer donor atoms such as are in the polyimide imide functionality. Polymer–metal coordination should be of pivotal importance in preventing the migration of metal(III) complexes to the surface of the film during thermal curing. Such metal–polymer coordination, or 'site isolation', has been suggested to lead to a uniform homogeneous distribution of nanometer-sized metal-oxo clusters throughout the polymer matrix [46–49]. Finally, we chose $[La(acac)_3(H_2O)_2]$ because unpublished X-ray data were disclosed which demonstrate that $[La(acac)_3(H_2O)_2]$ is transformed, with the loss of 2,4-pentanedione and water, by mild heating (75–85 °C) to a tetranuclear 2,4-pentanedionate complex, $[La_4(O)(acac)_{10}]$ with a tetrahedral $La_4(\mu_4\text{–}O)$ core [50]; this is consistent with several recent reports of the 'unexplained appearance of' and 'incorporation of unexpected' μ-oxo $[O^{2-}]$ groups [51] as polynuclear $M_x(\mu_x\text{–}O)$ cores formed particularly with oxophilic (lanthanides and actinides, and early transition elements) metal alkoxides. μ-Oxo ligands appear to be formed by hydrolysis and by thermally promoted cleavage of alkoxide C–O bonds, and their presence can be rationalized as 'a means of ensuring high coordination as encapsulated ligands in closo polyhedra' [51]. Thus, with $[La_4(O)\ (acac)_{10}]$ formed from $[La(acac)_3(H_2O)_2]$ we have a facile path to an initial metal-oxo phase.

The scattering diagrams of La_2O_3-6FDA/1,3(3)-APB polymer system are displayed in Fig. 2 as a function of a 100–300 °C 2 h ramp. Films were taken out of the oven during the ramp at the indicated temperature and analyzed via SAXS. It is evident from Fig. 2 that the nanoparticle formation begins to occur during the temperature ramp from 100 to 300 °C between 150 and 200 °C. The majority of the nanoparticle development occurs in the period during which the temperature increases from 200 to 250 °C. Films heated up to 200 °C only scatter in the lower q-range, but the nanostructure development is clear for the films heated taken out at 250 °C during the temperature ramp. The nanostructured films exhibit a clear correlation peak that shifts from about 0.06–0.052 $Å^{-1}$ with increasing cure temperature. The Beaucage [52] approach was applied in order to analyze these morphologies in terms of characteristic distances through the gyration radius of the nanoparticles, R_g, and the average distance between particles centers d. The results are given in Table 1. Both d and R_g increase slightly with cure time/temperature. Moreover, the increase of the parameter k clearly indicates an increase of the regularity in the packing of the particles with increasing cure time.

We also observe that the location of the correlation halo in the q-range is only slightly affected during curing, which is an indication that the formation of the nanoparticles could originate from: (1) a phase separation process with spinodal decomposition (possibly induced by the degradation of the lanthanum(III) complex or additional imidization) or (2) a nucleation/growth process with a high nucleation rate and thus controlled by the degradation of the lanthanum(III) complex.

A particularly important observation of the kinetics of particle formation process as observed in the SAXS results is that it should be possible to quench the formation process at various times and temperatures. Thereby a series of lanthanum(III) oxide nanoparticles in this polyimide system can be created in which the particle size and resulting interparticle distance varies. This will make it possible in future work to study the effect of the particle size on properties. Further it will then be possible to repeat such studies in which the chemical identity of the nanoparticle is varied and finally the chemical structure of the polyimide and other high temperature thermal plastics are changed.

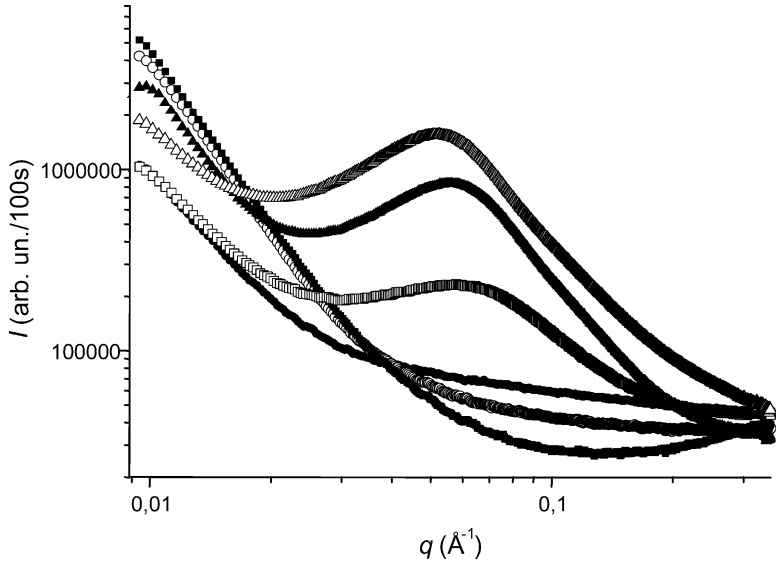

Fig. 2. Scattering diagrams of La-based hybrids for different curing temperatures, (●) 100 °C, (○) 150 °C, (¦)200 °C, (□) 250 °C, (▲) 300 °C, (△) 300 °C during 1 h.

Table 1
Results of the analysis of the scattering diagrams of Fig. 2 using the semi-phenomenological model of Beaucage [52]

Curing temperature	R_g (Å), gyration radius	d (Å), Interparticle distance	k, Packing order parameter
200 °C –□–	19	80	1
300 °C—1 h –△–	24	97	2.45

The nanoparticle formation process was also monitored during a 100–300 °C 2 h ramp using frequency dependent dielectric measurements over a range of frequencies from 50 Hz to 500 kHz. In order to interpret these results and to separate the effect of the nanoparticle formation process out from changes in the polymer itself, runs were made on both the doped and the neat polymer system. These results are shown in Fig. 3(A) and (B)—for the dielectric measurements. Here the neat system shows a distinct decrease in the ionic mobility during the temperature ramp from 150 to 200 °C. This is followed by an increase in the ionic mobility as the system becomes more fluid and the temperature rises above T_g. On the other hand, in the lanthanum(III) system this decrease in ionic mobility occurs at a distinctly higher temperature, 190–240 °C, reflecting the additional process of the lanthanum(III) complex degradation, the diffusion fed growth of the lanthanum(III) oxide nanoparticles and the increase in T_g due to the presence of the nanoparticle.

It was difficult to detect distinct differences between the neat and doped polyimide using a modulated differential scanning calorimeter. The nanoparticles formation process is not sufficiently thermally significant to produce a detectable signal. This is probably because of the small amount of sample in a DSC experiment and because the amount of dopant in the system is below 5%.

3.2. Characterization of the fully cured film

The TEM and SEM images of the La_2O_3-6FDA/1,3(3)-APB hybrid film after the final cure (300 °C) is seen in Fig. 4. The TEM image shows that discrete nanoparticle diameters are predominantly 3–8 nm; the SEM image is consistent with this size range. The micrographs are in reasonable agreement with the SAXS analysis (Table 1). Of particular importance, the particles are uniformly distributed within the polymer with characteristic interparticular distances of the order of 10 nm. Again, this is in agreement with the correlation peak exhibited by the SAXS scattering diagrams.

The final structure of the nanoparticles has also been studied by XPS measurements. The results show two pairs of lines indicating there are two distinct types of lanthanum(III) ions in the nanoparticles. The spectrum (Fig. 5) shows the expected $d_{5/2}$ and $d_{3/2}$ splitting for lanthanum with a separation of 16.8 eV suggesting two different lanthanum(III) environments.

3.3. Characterization of final physical properties

A traditional characterization of interaction between polymer and filler in nanostructured or confined systems is the change in the glass transition temperature. We have characterized the glass transition in the La_2O_3 nanoparticle polyimide (300 °C/1 h) and in the neat polyimide systems after identical thermal treatments. First both the neat and La films were heated to 250 °C at 2 °C/min with a 1 °C/min modulation. Then both films were cooled and reheated at the same rate. The neat film had a glass transition range as determined by the TA DSC software of 199.6–204.5 °C while the La_2O_3 polyimide film had a range of 201.5–208.1 °C range. The point of maximum change in heat flow is 202.7 °C for the neat film and 205.5 °C for the La_2O_3 containing film. There is also a significant decrease in the heat capacity of the lanthanum(III) oxide nanoparticle system compared to the neat polyimide. Clearly the high interactions between the PI matrix and lanthanum(III) oxide nanoparticles cause the glass transition to occur at a higher temperature and the glass transition range is considerably broader. This suggests that the La_2O_3 nanoparticles produce a broader range of environments for the polyimide chains, inducing a more heterogeneous glass transition dynamics. This is undoubtedly due in part to variations in mobility near the nanoparticle's surface relative those to chain segments further removed from the particles.

The effects of nanoparticles were also evaluated on the gas transport properties (Fig. 6). The permeability coefficients P_{H2} and P_{CO2} were measured on films prepared with different amounts of La_2O_3, derived from $La(acac)_3(H_2O)_2$, and their values are reported in Table 2. The diffusion coefficient was also determined on the different films for CO_2 (Table 2). It could not be calculated for H_2 because the time lag was too small for this gas. The precision on P and D values are, respectively, 0.02 barrer and 0.02 10^{-9} cm^2 s^{-1}.

The P_{H2}, P_{CO2} and D_{CO2} are each reduced with increasing metal content in the film (Table 2). The decrease of the gas permeability coefficient expressed as the ratio of

Table 2
Gas transport properties of the nanocomposites

Metal content in the film (wt%)	P_{H2} (barrer)	P_{CO2} (barrer)	D_{CO2} (10^{-9} cm^2 s^{-1})
0	8.42	1.48	1.29
1.79	7.86	1.39	1.18
3.02	7.25	1.27	1.10
4.64	7.16	1.23	1.06

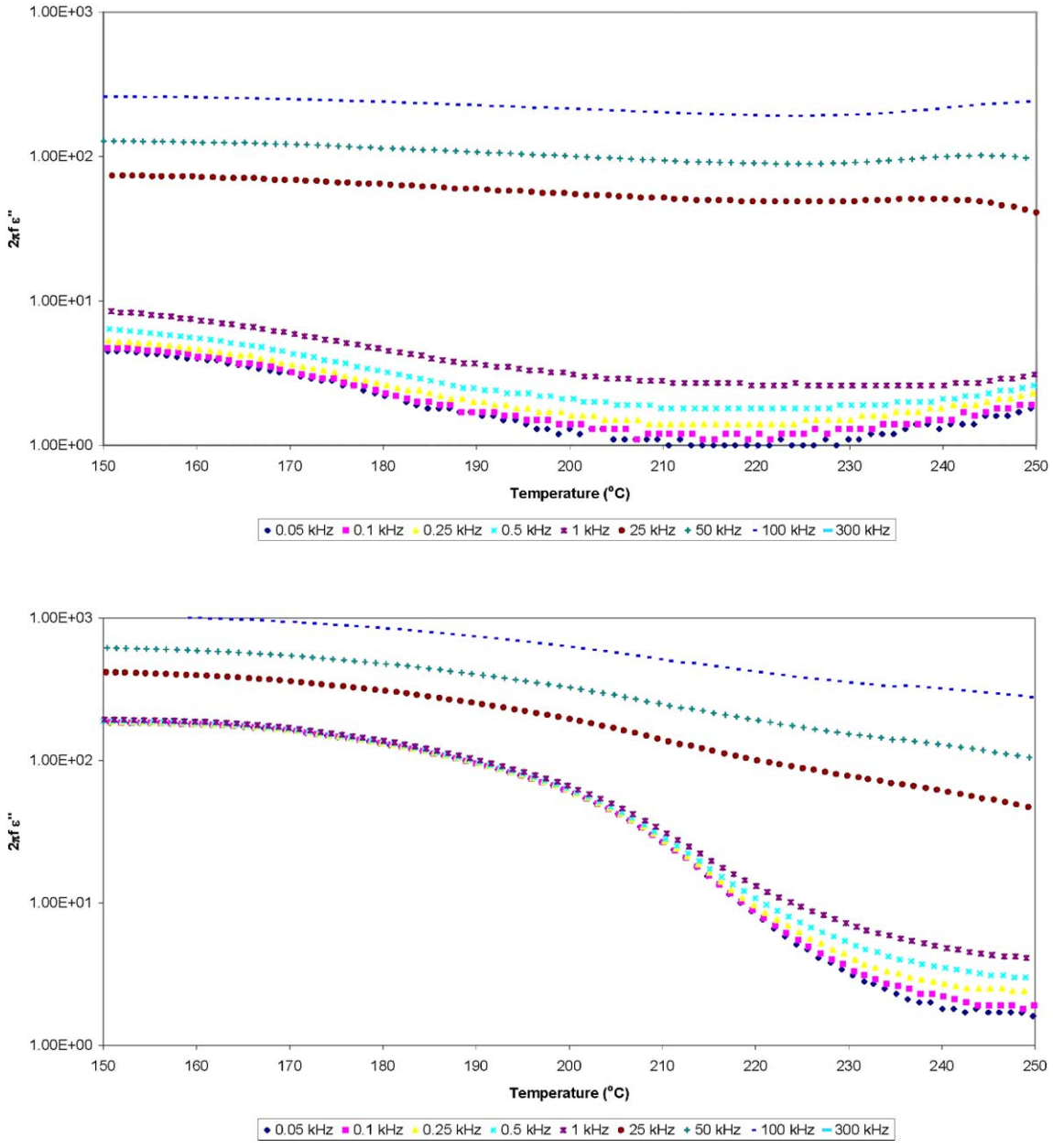

Fig. 3. (A) Dielectric spectroscopy values of the frequency times loss vs. temperature for the neat polyimide; overlapping lines are monitoring changes in ionic mobility. (B) Dielectric spectroscopy values of the frequency time loss vs. temperature for the lanthanum (III)-doped polyimide; overlapping lines are monitoring changes in ionic mobility.

the permeability of the composite to the permeability of the neat matrix (e.g. the relative permeability) is quite similar for the two gases and it is identical to the decrease observed for the diffusion coefficient (Fig. 6 and 7). All these data are consistent with the nanoparticles acting as impermeable spheres and they show that the increase of the barrier properties is large, mainly related to a tortuosity effect.

The experimental decrease of permeability has been compared to the theoretical decrease calculated using Maxwell law [53]. This law (Eq. (1)), developed for systems composed of a permeable matrix in which are dispersed spherical impermeable spheres of micrometric size, defines the relative permeability as a function of the volume fraction of the dispersed phase.

$$\frac{P_{\text{composite}}}{P_{\text{matrix}}} = \frac{2(1-\phi_{\text{d}})}{2+\phi_{\text{d}}} \tag{1}$$

This equation has been used to describe the behavior of semi-crystalline polymers, for which the crystalline fraction is assumed to be represented by spheres, these last ones being impermeable to gases [54]. It has also been used by Holsti-Miettinen et al. [55] for the study of polypropylene/polyamide six blends. The same equation has been obtained by Higuchi et al. [56] from the general equation he

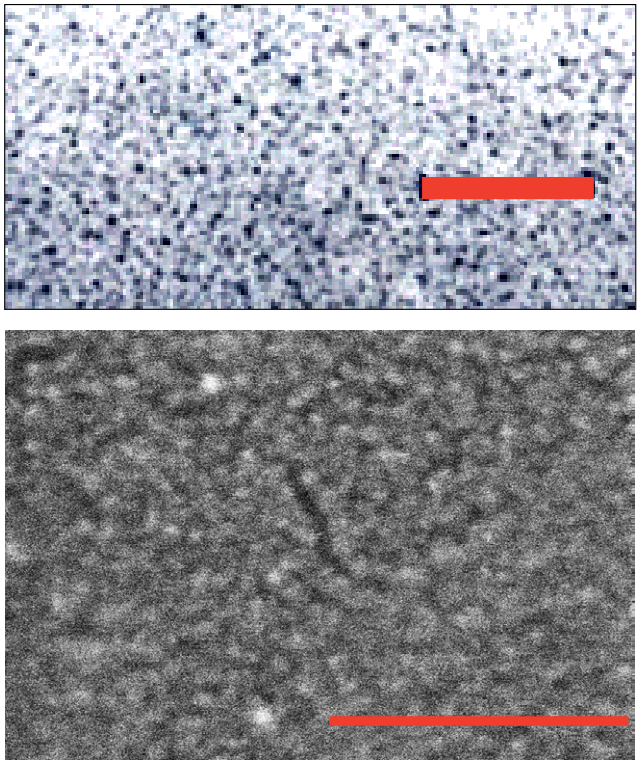

Fig. 4. TEM (top) and SEM (bottom) images of fully cured La_2O_3-6FDA/1,3(3)-APB hybrid cured to 300 °C for 1 h. The scale bars are 100 nm.

developed for blends for which the properties of either components phase are not altered by the presence of the other phase. According to Peterson [57], this equation is valid for relatively low volume fraction of the dispersed phase ($\phi_d < 0.3$). Nevertheless, a good agreement between theoretical and experimental permeability coefficients has been observed for a volume fraction of the dispersed phase equal to 0.5 and this result is explained by a high degree of agglomeration of the dispersed particles creating small

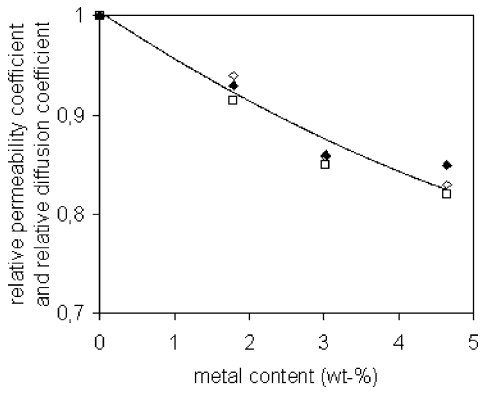

Fig. 6. Evolution of the relative permeability (the permeability of the composite ratioed to the permeability of the meat matrix for (□) H_2 and (□) CO_2 and of the (□) CO_2 relative diffusion as a function of the metal content in the film).

clusters of internal phase separated from neighboring clusters by relatively large distances.

According to this law, a permeability decrease of 15% that is experimentally observed with 1 vol% metal oxide nanoparticle content, corresponds to a theoretical volume percent, ϕ_d value, equal to 10%. Thus the decrease in permeability is ten times that predicted by the Maxwell model.

We have calculated the actual volume fraction of the particles to be 1.0% considering that they are exclusively composed of La_2O_3. Indeed, La 3d XPS regions have evidenced two different lanthanum(III) environments, but this can be attributed to the very small inorganic phase particle sizes which could lead both to interior and surface different lanthanum(III) species. Furthermore, the SAXS morphological analysis has confirmed the low value of the dispersed phase volume fraction. Thus the effect of the 1.0% volume fraction of La_2O_3 nanoparticles is ten times the theoretically predicted result.

In conclusion, an important barrier effect is evidenced compared to the theoretical Maxwell prediction. It could be

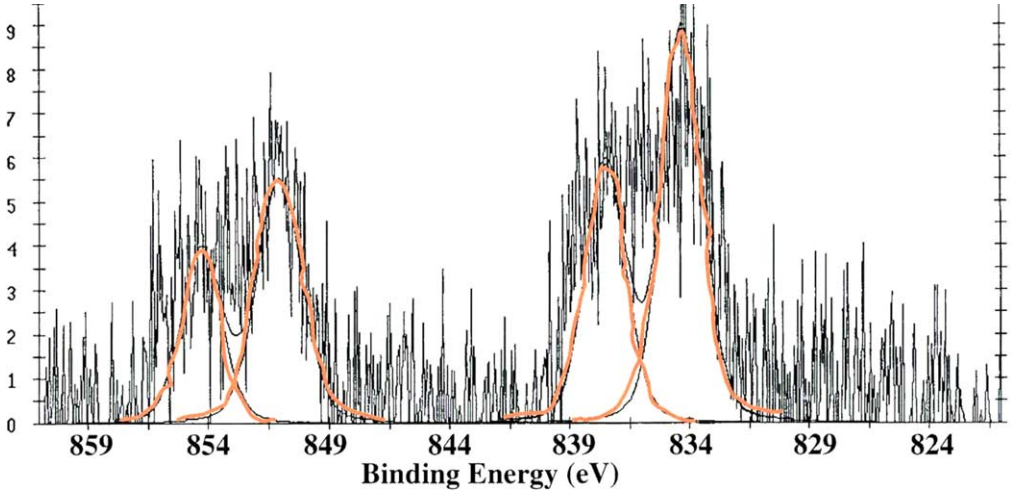

Fig. 5. XPS spectrum in the La (3d3/2 and 3d5/2) region for the La_2O_3-6FDA/1,3(3)-APB polyimide film cured to 300 °C for 1 h. La_2O_3 concentration is 4.4%.

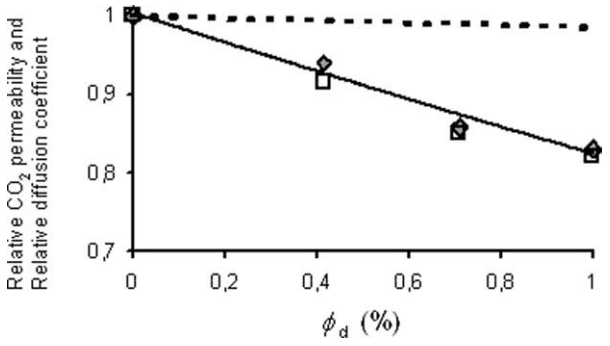

Fig. 7. Evolution of (□) the relative permeability (the permeability of the composite ratioed to the permeability of the neat matrix) and the (□) relative diffusion as a function of the nanoparticle volume fraction. The dotted line represents the expected values based on the Maxwell law.

attributed to two factors: (1) a higher tortuosity effect than that predicted by the law due to the very small size of the dispersed particles and to the low distance between the particles and (2) a restriction of the polymer chain mobility near the particles as underlined by dielectric and glass transition analysis. Thus an interesting and particularly sensitive measure of the nanoparticle interaction with the polyimide chains, we believe, are the gas permeability results. A distinct tortuosity effect is suggested when comparing the permeability of the lanthanum(III) oxide nanoparticle film to the permeability of the neat film and to the values obtained with the Maxwell law which is based on volume percent spherical impermeable particles.

4. Conclusions

An in situ and single-step route for creating a uniform dispersion of lanthanum(III) oxide nanoparticles in a polyimide has been described. The process of thermally evolving, from the diaquotris(2,4-pentanedionato)lanthanum(III) complex, 41 a homogeneous dispersion of lanthanum(III) oxide nanoparticles within a 6FDA/1,3(3)-APB polyimide matrix has been characterized using SAXS. The average radius of gyration of the newly formed nanoparticles was 2.4 nm and the average interparticle distance was 9.7 nm. Both the SAXS and the dielectric measurements indicate that the particles were formed as the temperature increased from 150 to 300 °C during a 2 h ramp from 100 to 300 °C. The development began as the temperature increased beyond 150 °C and the major development occurred by the time the temperature reached 250 °C. The resulting changes in the final properties of the 1% by volume nanoparticles in the polymer material relative to the neat polyimide indicate an increase in the glass transition temperature of 3 °C. Particularly important, the gas permeability showed a strong tortuosity effect due to the presence of 1% volume of the nanoparticles. The gas permeability was reduced by a factor of 10 compared with the predicted reduction of the Maxwell model. Characterization by X-ray photoelectron spectroscopy showed the lanthanum ions exist in two different chemical environments in the nanoparticle.

Acknowledgements

D. W. Thompson thanks the Petroleum Research Fund and Jeffress Memorial Trust for partial support of this work.

References

[1] Ahmad Z, Mark JE. Polyimide–ceramic hybrid composites by the sol–gel route. Chem Mater 2001;13:3320–30.
[2] Bian L-J, Qian X-F, Yin J, Zhu Z-K, Lu Q-H. Eu3+ complex/polyimide nanocomposites: improvement in mechanical and thermal properties. J Appl Polym Sci 2002;86:2707–12.
[3] Chiang P-C, Whang W-T, Tsai M-H, Wu S-C. Physical and mechanical properties of polyimide/titania hybrid films. Thin Solid Films 2004;447/448:359–64.
[4] Thompson DS, Thompson DW, Southward RE. In: Swift G, Carraher CE, editors. Functional condensation polymers. New York: Kluwer; 2002. p. 3–15.
[5] Thompson DS, Thompson DW, Southward RE. Oxo-metal–polyimide nanocomposites. 2. Enhancement of thermal, mechanical, and chemical properties in soluble hexafluoroisopropylidene-based polyimides via the in situ formation of oxo-lanthanide(III)-polyimide nanocomposites. Chem Mater 2002;14:30–7.
[6] Southward RE, Thompson DS, Thornton TA, Thompson DW, Clair St AK. Enhancement of dimensional stability in soluble fluorinated polyimides via the in situ formation of lanthanum(III)-oxo-polyimide nanocomposites. Chem Mater 1998;10:486–94.
[7] Southward RE, Thompson DS, Thompson DW, Clair St AK. Enhancement of dimensional stability in soluble polyimides via lanthanide(III) acetate additives. J Adv Mater 1996;27:2–8.
[8] Southward RE, Thompson DS, Thompson DW, Clair St AK. In: Pittman CU, Carraher CE, Culbertson BM, Zeldin M, Sheets JE, editors. Metal-containing polymeric materials. New York: Plenum; 1996. p. 337–47.
[9] Agag T, Koga T, Takeichi T. Studies on thermal and mechanical properties of polyimide–clay nanocomposites. Polymer 2001;42:3399–408.
[10] Chisholm BJ, Moore RB, Barber G, Khouri F, Hempstead A, Larsen M, et al. Nanocomposites derived from sulfonated poly(butylene terephthalate). Macromolecules 2002;35:5508–16.
[11] Fukushima Y, Inagaki S. Synthesis of an intercalated compound of montmorillonite and 6-polyamide. J Inclusion Phenom 1987;5:473–82.
[12] Fukushima Y, Okada A, Kawasumi M, Kurauchi T, Kamigaito O. Swelling behavior of montmorillonite by polyamide 6. Clay Miner 1988;23:27–34.
[13] Gilman JW. Flammability and thermal stability studies of polymer layered-silicate (clay) nanocomposites. Appl Clay Sci 1999;15:31–49.
[14] Gu A, Chang F-C. A novel preparation of polyimide/clay hybrid films with low coefficient of thermal expansion. J Appl Polym Sci 2000;79:289–94.
[15] Gu A, Kuo S-W, Chang F-C. Syntheses and properties of PI/clay hybrids. J Appl Polym Sci 2001;79:1902–10.
[16] Hsiao S-H, Liou G-S, Chang L-M. Synthesis and properties of organosoluble polyimide/clay hybrids. J Appl Polym Sci 2001;80:2067–72.

[17] Kojima Y, Usuki A, Kawasumi M, Okada A, Fukushima Y, Kurauchi T, et al. Mechanical properties of nylon 6-clay hybrid. J Mater Res 1993;8:1185–9.
[18] Kojima Y, Usuki A, Kawasumi M, Okada A, Kurauchi T, Kamigaito O. Synthesis of nylon 6-clay hybrid by montmorillonite intercalated with e-caprolactam. J Polym Sci Part A: Polym Chem 1993;31:983–6.
[19] Lan T, Kaviratna PD, Pinnavaia TJ. On the nature of polyimide–clay hybrid composites. Chem Mater 1994;6:573–5.
[20] LeBaron PC, Wang Z, Pinnavaia TJ. Polymer-layered silicate nanocomposites: an overview. Appl Clay Sci 1999;15:11–29.
[21] Morgan AB, Gilman JW, Jackson CL. Characterization of the dispersion of clay in a polyetherimide nanocomposite. Macromolecules 2001;34:2735–8.
[22] Tyan H-L, Liu Y-C, Wei K-H. Thermally and mechanically enhanced clay/polyimide nanocomposite via reactive organoclay. Chem Mater 1999;11:1942–7.
[23] Tyan H-L, Liu Y-C, Wei K-H. Enhancement of imidization of poly(amic acid) through forming poly(amic acid)/organoclay nanocomposites. Polymer 1999;40:4877–86.
[24] Yano K, Usuki A, Okada A. Synthesis and properties of polyimide–clay hybrid films. J Polym Sci Part A: Polym Chem 1997;35:2289–94.
[25] Yano K, Usuki A, Okada A, Kurauchi T, Kamigaito O. Synthesis and properties of polyimide–clay hybrid. J Polym Sci Part A: Polym Chem 1993;31:2493–8.
[26] Harris PJF. Carbon nanotube composites. Int Mater Rev 2004;49:31–43.
[27] Park C, Ounaies Z, Watson KA, Crooks RE, Smith J, Lowther SE, et al. Dispersion of single wall carbon nanotubes by in situ polymerization under sonication. Chem Phys Lett 2002;364:303–8.
[28] Park C, Ounaies Z, Watson KA, Pawlowski K, Lowther SE, Connell JW, et al. Polymer-single wall carbon nanotube composites for potential spacecraft applications. Mater Res Soc Symp Proc 2002;706:91–6.
[29] Smith Jr JG, Connell JW, Delozier DM, Lillehei PT, Watson KA, Lin Y, et al. Space durable polymer/carbon nanotube films for electrostatic charge mitigation. Polymer 2004;45:825–36.
[30] Watson KA, Smith Jr JG, Connell JW. Polyimide/carbon nanotube composite films for potential space applications. Int SAMPE Tech Conf 2001;33:1551–60.
[31] Watson KA, Smith Jr JG, Connell JW. Space durable polyimide/carbon nanotube composite films for electrostatic charge mitigation. Int SAMPE Symp Exhibition 2003;48:1145–55.
[32] Gaddy GA, Miner GA, Stoakley DM, Locke EP, Moore RL, Schultz J, et al. Optical and mechanical properties of photoassisted, self-assembled nanoparticle films. Mater Res Soc Symp Proc 2004;797:255–60.
[33] Gaddy GA, Miner GA, Stoakley DM, Locke EP, Schultz J, Moore RL. Method for the controlled formation and placement of metal layers in polyimide films. Polym Mater Sci Eng 2004;90:331–2.
[34] Southward RE. Metal–polyimide nanocomposite films. Part I. Single-stage synthesis of reflective and conductive silvered polyimide films for space applications prepared from (hexafluoroacetylacetonato) silver(I) and (trifluoroacetylacetonato)silver(I) with BTDA/4,4′-ODA. Met Plast 2001;7:143–69.
[35] Southward RE, Pevzner M, Thompson DW. Silver–polyimide nanocomposite membranes: self-generated highly reflective flexible mirrored surfaces. Mater Res Soc Symp Proc 2003;775:193–8.
[36] Southward RE, Thompson DW, Inverse CVD. A novel synthetic approach to metalized polymeric films. Adv Mater (Weinheim, Germany) 1999;11:1043–7.
[37] Southward RE, Thompson DW. Metal–polyimide nanocomposite films. Part II. The effects of the silver(I) ligand, polymer viscosity, and polymer structure on the single-stage synthesis of surface silvered polyimide films. Met Plast 2001;7:171–88.
[38] Southward RE, Thompson DW. Metal–polyimide nanocomposite films: single-stage synthesis of silvered polyimide films prepared from silver(I) complexes and BPDA/4,4′-ODA. Chem Mater 2004;16:1277–84.
[39] Clair St AK, Carver VC, Taylor LT, Furtsch TA. Pd//electrically conductive polyimide films containing palladium coordination complexes. J Am Chem Soc 1980;102:876–8.
[40] Stoakley DM, Clair St AK. Low coefficient of thermal expansion polyimides containing metal ion additives. SAMPE Q 1992;23:9–13.
[41] Phillips II T, Sands DE, Wagner WF. Crystal and molecular structure of diaquotris(acetylacetonato)lanthanum(III). Inorg Chem 1968;7:2295–9.
[42] Pope GW, Steinbach JF, Wagner WF. Characteristics of the solvates of the rare-earth acetyl-acetonates. J Inorg Nucl Chem 1961;20:304–13.
[43] Stites JG, McCarty CN, Quill LL. The rare earth metals and their compounds VIII. An improved method for the synthesis of some rare earth acetylacetonates. J Am Chem Soc 1948;70:3142–3.
[44] Shannon RD. Acta Crystallogr 1976;A32:751.
[45] Sinha SP. Structure and bonding in highly coordinated lanthanide complexes. Struct Bond 1976;25:69–149.
[46] Nandi M, Sen A. Chemical basis for adhesion. Interaction of chromium with polyimide: model studies. Chem Mater 1989;1:291.
[47] Nandi M, Conklin JA, Salvati L, Sen CM. Molecular level ceramic/polymer composites. 2. Synthesis of polymer-trapped silica and titania nanoclusters. Chem Mater 1991;3:201–6.
[48] Nandi M, Conklin JA, Salvati L, Sen A. Molecular level ceramic/polymer composites 1. Synthesis of polymer-trapped oxide nanoclusters of chromium and iron. Chem Mater 1990;2:772–6.
[49] Sen A, Nandi M, Conklin JA. Molecular level metal and ceramic/polymer composites: synthesis of metal and metal oxide containing polyimides and its relevance to polymer metallization. Met Plast 1992;2:35–55.
[50] McLain SJ. DuPont central research, disclosed at new organic chemistry for polymer synthesis, division of polymer chemistry. Santa Fe, NM: American Chemical Society; 1995.
[51] Caulton KG, Hubert-Pfalzgraf LG. Synthesis, structural principles and reactivity of heterometallic alkoxides. Chem Rev (Washington, DC, USA) 1990;90:969–95.
[52] Beaucage G, Schaefer DW. Structural studies of complex systems using small-angle scattering: a unified Guinier/power-law approach. J Non-Cryst Solids 1994;172–174:797–805.
[53] Barrer RM. In: Crank J, Park GS, editors. Diffusion in polymers, chapter 6, diffusion and permeation in heterogeneous media. New York: Academic Press; 1968.
[54] Orchard GAJ, Ward IM. The permeation of oxygen through drawn films of poly(ether ether ketone). Polymer 1992;33:4207–9.
[55] Holsti-Miettinen RM, Perttila KP, Seppala JV, Heino MT. Oxygen barrier properties of polypropylene/polyamide 6 blends. J Appl Polym Sci 1995;58:1551–60.
[56] Higuchi WI, Higuchi T. Theoretical analysis of diffusional movement through heterogeneous barriers. J Am Pharm Assoc Sci Ed 1960;49:598–606.
[57] Peterson CM. Permeability studies on heterogeneous polymer films. J Appl Polym Sci 1968;12:2649–67.